

# Low-Lying Electronic Excited States of Pentacene Oligomers: A Comparative Electronic Structure Study in the Context of Singlet Fission

Pedro B. Coto,<sup>\*,†</sup> Sahar Sharifzadeh,<sup>\*,‡,§,#</sup> Jeffrey B. Neaton,<sup>\*,‡,§,||</sup> and Michael Thoss<sup>\*,†</sup>

<sup>†</sup>Institut für Theoretische Physik und Interdisziplinäres Zentrum für Molekulare Materialien (ICMM), Friedrich-Alexander-Universität Erlangen-Nürnberg, Staudtstrasse 7/B2, D-91058 Erlangen, Germany

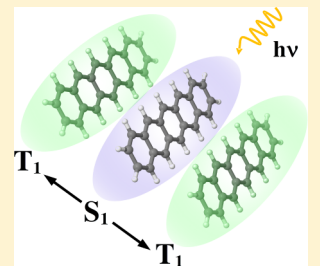
<sup>‡</sup>Molecular Foundry, Lawrence Berkeley National Laboratory, Berkeley, California 94720, United States

<sup>§</sup>Department of Physics, University of California, Berkeley, California 94720, United States

<sup>||</sup>Kavli Energy Nanosciences Institute at Berkeley, Berkeley, California 94720, United States

## Supporting Information

**ABSTRACT:** The lowest-lying electronic excited states of pentacene and its oligomers are investigated using accurate multireference wave function methods (CASPT2/CASSCF) and the many-body Greens's function approach (GW/BSE). The results obtained for dimers and trimers of different geometry reveal a complex electronic structure, which includes locally excited, charge transfer, and multiexciton states. For singlets of single-excitation character, both approaches yield excitation energies that are in good overall quantitative agreement. While the multiexciton states are located relatively high in energy in all systems investigated, charge transfer states exist in close proximity to the lowest-lying absorbing states. The implications of the results for the mechanisms of singlet fission in pentacene are discussed.



## 1. INTRODUCTION

Singlet fission (SF) in organic materials is a mechanism where two triplet excitons are formed after photoexcitation of one singlet exciton through a spin-allowed process.<sup>1,2</sup> It has received great attention recently<sup>3–12</sup> as a possible mechanism to increase the efficiency of solar cells beyond the Shockley–Queisser limit.<sup>13</sup> Although the formation of triplet states via SF in crystals and thin films of organic molecules has been known for many decades<sup>14–24</sup> and several theoretical models have been proposed to rationalize the process,<sup>25–29</sup> the detailed mechanism of SF is still a controversial topic. Recent works have focused on two important aspects. The first concerns the search for molecules that exhibit SF.<sup>1–3,30–32</sup> Molecules suitable for SF have to fulfill the energy criteria

$$2E(T_1) - E(S_1) \lesssim 0 \quad (1)$$

$$2E(T_1) - E(T_2) \leq 0 \quad (2)$$

for the involved electronic states.<sup>1,3</sup> Thereby, the first relation ensures that the splitting of the initially excited singlet exciton ( $S_1$ ) into two triplet excitons ( $T_1$ ) is an exoergic process. The second relation indicates that the energy difference between the lowest-lying states in the triplet manifold has to be large enough to minimize triplet–triplet annihilation. Based on these energy criteria, Michl and co-workers<sup>1,33</sup> have suggested the use of molecules derived from large alternant  $\pi$ -conjugated hydrocarbons or small biradicaloid heterocycles (both having high absorption coefficients in the visible region of the electromagnetic spectrum) in SF based solar cells.

The second aspect that has been the subject of intense research recently is the elucidation of the SF mechanism at the molecular level. This requires the determination of the electronic states involved in the process, the coupling mechanisms between them, the effect of nuclear dynamics and also an accurate understanding of the molecular-scale morphology and its impact on these quantities. In most of the recent works on this topic,<sup>1,34–49</sup> two mechanisms are invoked to rationalize the process of SF, the direct and the two-step mechanism. Both differ in the number and character of the involved electronic states and, therefore, in the kinetic model. In the direct mechanism, the initially excited bright state transforms directly via nonradiative decay into a correlated triplet pair state, denoted by  ${}^1(T_1T_1)$ . The  ${}^1(T_1T_1)$  state, which is also called multiexcitonic (ME) or doubly excited (D) state, is formally a singlet state build from two triplet states localized at different molecules. In the two-step mechanism, on the other hand, the bright state decays via an intermediate state to the ME state. The intermediate state typically shows charge transfer (CT) character. Depending on symmetry it may or may not exhibit a permanent dipole moment. States that due to symmetry lack a permanent dipole moment but with wave functions involving CT configuration state functions (CSFs) are sometimes called charge resonance states. For ease of notation, in this work, we will use the label CT also for this type of states. Some recent works<sup>8,43,46</sup> have challenged both mechanisms and suggested that light absorption results in a

Received: June 11, 2014

Published: December 9, 2014



coherent superposition of the bright and ME states. In all cases, the ME state dissociates ultimately into two separated triplet states. The prevalence of one or the other mechanism may also depend on the specific system under consideration.

In this work, we consider pentacene, a paradigm molecule for SF. As a prerequisite for the elucidation of the SF mechanism, we characterize the low-lying electronically excited states of pentacene and several oligomers using two different approaches: high-level ab initio multireference perturbation theory employing the CASPT2/CASSCF approach as well as many-body perturbation theory based on the GW approach and the Bethe–Salpeter equation (GW/BSE). In this work, we focus on the analysis of the adiabatic electronic states. These form the basis where the electronic Hamiltonian is diagonal, and they are coupled nonadiabatically via the derivative coupling. They differ from the diabatic states usually employed in the investigation of the dynamics of the SF which are coupled via the nondiagonal elements of the electronic Hamiltonian.

Specifically, we consider the pentacene oligomers depicted in Figure 1, which are characterized by different geometrical

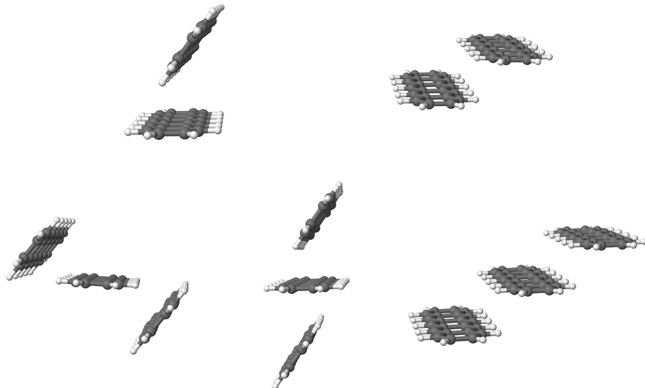


**Figure 1.** Different dimers and trimers of pentacene investigated in this work. Top: herringbone-like dimer (left) and parallel C<sub>1</sub> dimer (right). Bottom: herringbone-like trimer conformations HS-1 (left) and HS-2 (center), and parallel symmetric trimers (right).

conformations. The reasons for the selection of these specific conformations are twofold. On the one hand, the use of oligomers of increasing size provides a way of improving the description of the delocalized character of the low-lying excited states. As it has recently been shown,<sup>50,51</sup> the lowest singlet exciton found in the S-phase crystal structure of pentacene exhibits a delocalized character extending over several pentacene units. Therefore, the adequate description of this state requires cluster models at least larger than dimers. In addition, trimers allow the characterization of the electronic states in different geometrical conformations consistent with the symmetry of the pentacene crystal.

## 2. COMPUTATIONAL METHODS

We have considered the pentacene systems depicted in Figure 1, including the monomer as well as several dimers and trimers with different geometrical conformations taken from the optimized S-phase crystal structure reported in ref 50. To characterize the lowest-lying electronically excited singlet states of these systems, we have employed two different theoretical methods, GW/BSE and CASPT2/CASSCF. While the former method is applicable to extended systems and has recently been

used to study pentacene crystals,<sup>50,51</sup> the latter is a multi-reference method that allows a balanced description of electronic states of very different nature,<sup>52</sup> including states with multiple excitations. The comparison of the results, therefore, provides also a benchmark of the two approaches for the present systems.

The GW/BSE method has been employed to characterize the lowest-lying singlet electronic excited states of pentacene and the two dimers shown in Figure 1. The GW calculations are based on a standard G<sub>0</sub>W<sub>0</sub> scheme, where quasi-particle energies are computed via a first-order correction to density functional theory (DFT) eigenvalues, with no self-consistent update of the starting wave functions. The static dielectric function has been computed within the random-phase approximation and extended to finite frequency via the generalized plasmon-pole (GPP) model of Hybertsen and Louie.<sup>53</sup> Given the static inverse dielectric function and quasiparticle energies, neutral excitations are computed via the solution of the Bethe–Salpeter equation (BSE). We use an approximate form of the BSE developed within an ab initio framework by Rohlfsing and Louie, which uses the Tamm–Danoff and static kernel approximations.<sup>54</sup> The starting eigenvalues and eigenvectors for GW were computed at the DFT level employing the PBE correlation-exchange functional<sup>55</sup> with the Quantum Espresso package.<sup>56</sup> The nuclei and core electrons were described using Troullier–Martins relativistic norm-conserving pseudopotentials.<sup>57</sup> In our pseudopotentials, 1 (4) electrons were explicitly considered as valence electrons for H (C), with cutoff radii of 1.0 (1.3) au. Following previous studies,<sup>50</sup> the planewave energy cutoff for the DFT calculations was 680 eV, sufficient to converge the total energy to <10 meV/atom. The GW self-energy and dielectric function were computed as a truncated sum over empty states. For the pentacene monomer, the sum was truncated at 30 eV above the vacuum level<sup>50</sup> whereas due to the computational cost, the sum was truncated at 24 eV for the dimers. The dielectric function planewave cutoff was 140 eV. To avoid spurious interactions with periodic images, the molecules were placed in a supercell with lattice vectors set to twice the size necessary to contain 99% of the charge density and the Coulomb interaction was truncated at distances larger than half of the unit cell size. The supercell dimensions, in atomic units, were 60 × 30 × 10, 36 × 47 × 58, and 47 × 33 × 61 for the pentacene molecule, herringbone structure dimer, and face-to-face structure dimer, respectively. The BSE sum was computed using 5 (10) valence × 5 (10) conduction states for the molecule (dimer). All GW calculations were carried out using the BerkeleyGW package.<sup>58</sup>

The CASPT2/CASSCF calculations have been carried out using state-average (SA) CASSCF wave functions as reference (see Supporting Information for further details). The quality of the CASPT2/CASSCF calculations depends on the choice of the active space. Ideally, for the systems investigated, the full π-system should be included in the CASSCF calculation, but this is computationally intractable. On the other hand, too small active spaces may lead to numerical and sometimes qualitative inaccuracies. We have performed extensive tests to assess the quality of the results for the electronic states of interest with respect to the variation of the size of the active space (see Supporting Information). Specifically, in the case of pentacene we have employed an active space of 14 electrons in 14 π-like orbitals (14e<sup>-</sup>/14o) together with an ANO-L basis set<sup>59</sup> with the primitive set C(14s9p4d3f)/H(8s4p3d) contracted to

$C[4s3p2d1f]/H[3s2p1d]$  as reference. This level of theory was used to assess the accuracy of the results obtained with a smaller active space ( $4e-/4o$ ) and basis set (ANO-S<sup>60</sup> with primitive set  $C(10s6p3d)/H(7s3p)$  contracted to  $C[3s2p1d]/H[2s1p]$ ). The choice  $4e-/4o$  is the minimum set of orbitals per pentacene unit needed to describe the electronic states involved in SF in dimers ( $8e-/8o$ ) and trimers ( $12e-/12o$ ). The ANO-S basis set of double- $\zeta$  quality allows a reasonable balance between accuracy and computational cost. Additional tests have been performed for the example of the pentacene dimer in herringbone configuration (see Supporting Information). The results for this system show that active spaces that are computationally affordable provide a description of the lowest lying electronic excited states within the typical accuracy of the method ( $\sim 0.2$  eV).<sup>52</sup> Higher lying states and scans of their potential energy surface, on the other hand, may require in some cases significantly larger active spaces.

The CASPT2 energies were computed using a zero-order Hamiltonian that includes the IPEA (0.25 au) shift.<sup>61</sup> To avoid the effects of intruder states an imaginary level-shift of 0.1 au was also used.<sup>62</sup> Oscillator strengths were computed using the CASSCF transition dipole moments and the CASPT2 energy differences. All the calculations were carried out using MOLCAS 7.8.<sup>63</sup>

### 3. RESULTS AND DISCUSSION

In this section, we report the results obtained in the characterization of the lowest-lying singlet excited states for the cluster models shown in Figure 1 using the methodologies detailed in the previous section.

**3.1. Pentacene Monomer.** Table 1 shows the vertical excitation energies, symmetry, oscillator strengths, and natural

**Table 1. Vertical Excitation Energies [CASPT2/SA-CASSCF(14,14)/ANO-L-VTZP, in eV], Oscillator Strengths, and Natural Orbitals with Significant Changes in Occupation Numbers of the Three Lowest-Lying Singlet Excited Electronic States of Pentacene<sup>a</sup>**

State	$\Delta E$	f	Natural Orbitals
$S_1 (B_{2u})$	2.31	0.102	
$S_2 (A_g)$	2.88	0.000	
$S_3 (B_{3u})$	3.14	0.077	

<sup>a</sup> $D_{2h}$  symmetry was used in the calculations. The double arrow indicates that the state has a significant contribution of doubly excited configurations

orbitals (NO) with significant changes in occupation numbers of the lowest-lying singlet excited electronic states of pentacene computed using the CASPT2/CASSCF/ANO-L-VTZP method. The molecular geometry was taken from the optimized crystal structure reported in ref 50. The calculations were carried out enforcing  $D_{2h}$  symmetry and using an  $14e-/14o$  active space together with a triple- $\zeta$  ANO-L basis set (see Methods and Supporting Information for details). The results show that the lowest-lying singlet excited state ( $S_1$ ) is a bright state of  $B_{2u}$  symmetry ( $^1L_a$ , short axis-polarized) located 2.31 eV above the ground state ( $X^1A_g$ ). This state is well described in terms of a single configuration and mainly involves the

transition of a single electron between the NOs shown in Table 1. The second lowest-lying singlet excited state ( $S_2$ ) is dark in absorption, has  $A_g$  symmetry, and is found 2.88 eV above the ground state. It has multiconfigurational character, with dominant configuration state functions (CSFs) involving double excitations and the NOs shown in Table 1. Finally, the third lowest-lying singlet state ( $S_3$ ) is bright in absorption, has  $^1B_{3u}$  symmetry ( $^1L_b$ , long axis-polarized), and is located 3.13 eV above the ground state. It can be described in terms of two CSFs involving single excitations and the NOs depicted in Table 1.

The results of the GW/BSE method for the pentacene monomer are depicted in Table 2. For the bright states ( $S_1$  and

**Table 2. Vertical Excitation Energies (GW/BSE, in eV) and Most Significant Single Excitation Contributions of the Three Lowest-Lying Singlet Excited Electronic States of Pentacene<sup>a</sup>**

State	$\Delta E$	Most Significant Single Excitations
$S_1$	2.20	
$S_2$	2.80	
$S_3$	3.07	

<sup>a</sup>Symmetry was not used in the calculations.

$S_3$ ,  $^1B_{2u}$  and  $^1B_{3u}$  respectively), the agreement with the CASPT2 results is very good in terms of state ordering, excitation energies, and character of the states (see Table 2). Discrepancies appear in the nature of  $S_2$ . Instead of an  $A_g$ -like state with similar characteristics as that obtained with CASPT2, GW/BSE predicts a  $S_2$  state of  $B_{1g}$  symmetry with vertical excitation energy very similar to the  $2^1A_g$  state found at the CASPT2 level (see Tables 1 and 2). This difference is due to the known limitations of the GW/BSE method used in describing doubly excited configurations; such configurations are beyond the scope of the GW/BSE approach used here.<sup>64</sup>

The CASPT2 results agree well with the available experimental data for the lowest-lying absorbing state. In particular, the values obtained for the vertical excitation energies of the bright  $S_1$  state are in very good agreement with the  $S_1 \leftarrow S_0$  0–0 transition found in the absorption spectra of pentacene in the gas phase (2.31 eV).<sup>65</sup> Furthermore, they also agree with the maximum of the absorption spectra found for pentacene in Ne (2.28 eV), Ar (2.21 eV), and Kr (2.19 eV) matrices.<sup>66</sup> For the next bright state  $S_3$  our results differ appreciably ( $\sim 0.5$  eV) from those reported in ref 66 that we tentatively assign to a  $2^1B_{3u}$  state on the basis of the CASPT2 calculations (see Supporting Information). Finally, our results are also in agreement with estimates of the vertical excitation

**Table 3.** Vertical Excitation Energies [CASPT2/SA-CASSCF(8,8)/ANO-S-VDZP, in eV], Oscillator Strengths, Modulus of the Dipole Moments<sup>a</sup> (D), Character of the States, Density Difference Plots, and Natural Orbitals with Significant Changes in Occupation Numbers of the Five Lowest-Lying Singlet Excited Electronic States of the Pentacene Herringbone Dimer<sup>b</sup>

State	$\Delta E$	f	$ \mu $	Character	Density Difference	Natural Orbitals
S <sub>1</sub>	2.22	0.092	13.246	CT		
S <sub>2</sub>	2.37	0.083	3.807	LE		
S <sub>3</sub>	2.43	<0.001	1.733	ME		
S <sub>4</sub>	2.55	0.003	23.256	CT		
S <sub>5</sub>	2.56	0.089	4.903	LE		

<sup>a</sup>The modulus of the dipole moment of the ground state is 1.249 D. <sup>b</sup>Density differences and natural orbitals were computed at the SA-CASSCF(8,8)/ANO-S-VDZP level. In the density difference plots the yellow indicates accumulation and blue depletion of electronic density, respectively (an isolevel value of 0.0003 au was used in the plots).

energies derived by Grimme and Parac (2.37 and 3.12 eV) from experimental 0–0 transition energies in solution.<sup>67</sup>

A variety of other theoretical methods have been applied to characterize the electronic spectrum of pentacene. Grimme and Parac<sup>67,68</sup> used CC2 to calculate the vertical excitation energies for the L<sub>a</sub> (2.35 eV) and L<sub>b</sub> (3.27 eV) bright states, obtaining values similar to those reported in this work. However, they did not report any value for the 2<sup>1</sup>A<sub>g</sub> state. More recently, Marian et al.<sup>69</sup> carried out a comprehensive study of the lowest-lying excited electronic states of pentacene at the DFT/MRCI level of theory. The results obtained by these authors are in line with those obtained at the CASPT2 level both in the order of the states and also in their vertical excitation energies. The DFT/MRCI energies are very slightly red-shifted by 0.09 and 0.04 eV for the absorbing 1<sup>1</sup>B<sub>2u</sub> and 1<sup>1</sup>B<sub>3u</sub> states, respectively. This agreement also extends to the 2<sup>1</sup>A<sub>g</sub> state, which, according to ref 69, is located between the 1<sup>1</sup>B<sub>2u</sub> and 1<sup>1</sup>B<sub>3u</sub> states. For this state, the discrepancy between the DFT/MRCI and CASPT2 excitation energies is somewhat larger than for the S<sub>1</sub> and S<sub>3</sub> absorbing states, with the DFT/MRCI result showing a red-shift of 0.32 eV with respect to the CASPT2 value.

Knippenberg et al.<sup>70</sup> have also investigated the lowest-lying excited electronic states of pentacene. These authors used different versions of the ADC(2) method and found an ordering of the excited electronic states different from that obtained at the CASPT2 level. Specifically, the results differ in the location of the 2<sup>1</sup>A<sub>g</sub> state whose excitation energy deviates from that obtained at the CASPT2 level by as much as 1 or 2 eV depending on the ADC(2) version used. The situation is less dramatic for the excitation energies of the bright states 1<sup>1</sup>B<sub>2u</sub> and 1<sup>1</sup>B<sub>3u</sub>, where the ADC(2) results compare reasonably well with the CASPT2 values, with the former slightly blue-shifted by 0.15 and 0.23 eV, respectively.

Finally, Zimmerman et al.<sup>35</sup> and, more recently, Zeng et al.<sup>48</sup> investigated the lowest-lying electronic states of pentacene using multireference Moller–Plesset perturbation theory (MRMP). The value for the vertical excitation energy of the lowest-lying singlet state 1<sup>1</sup>B<sub>2u</sub> reported by Zeng et al. (2.31 eV) agrees with the value obtained by CASPT2, whereas the result of Zimmerman et al. (2.05 eV) is somewhat lower. More discrepancies appear in the vertical excitation energy of the dark 2<sup>1</sup>A<sub>g</sub> state. For this, the MRMP energies reported in both works show a red-shift with respect to the CASPT2 value of 0.93 and 0.25 eV, respectively. While the 0.25 eV red-shift can be the result of the different geometries of the pentacene models used in the calculations, the value of 0.93 eV seems to be an artifact caused by an intruder state problem.<sup>48</sup>

The aforementioned results point out that the lowest-lying singlet excited electronic states of pentacene can be described in a balanced and quite accurate way at the CASPT2 level using a relatively large active space and basis set. The same could be said for the GW/BSE method for electronic excited states that can be described in terms of single excitations, which are in good overall agreement with CASPT2. Calibration calculations (see Supporting Information) show that these results do not deteriorate significantly if a smaller active space and basis set are used. Calculations carried out using the ANO-S-VDZP basis set (primitive set C(10s6p3d)/H(7s3p) contracted to C-[3s2p1d]/H[2s1p]) and a reduced active space of 4e–/4o (including HOMO, HOMO–1, LUMO, and LUMO+1, see Supporting Information) indicate that this level of theory still provides a good description of the two lowest-lying excited states 1<sup>1</sup>B<sub>2u</sub> and 2<sup>1</sup>A<sub>g</sub> (see Supporting Information), a result that will be employed for the characterization of the lowest-lying electronic states of the dimers and trimers of pentacene. For higher lying states, inaccuracies in vertical excitation energies

can be expected to be significant and, in some cases, beyond the characteristic error of the method for this kind of molecule ( $\sim 0.2$  eV).<sup>52</sup> Furthermore, the results obtained for the monomer do not necessarily extrapolate to oligomers, in particular for intermolecular CT states. Therefore, we have used the GW/BSE method to further assess the reliability of the results obtained with the 8e-/8o active space in both dimers (see below). In addition, we have tested the stability of the CASPT2 results obtained for the herringbone-like dimer with respect to changes in the size of the active space (see Supporting Information for details).

**3.2. Pentacene Dimers and Trimers.** We have studied different dimers and trimers of pentacene with geometries obtained from the structure of the crystalline solid. Two types of arrangements have been considered, one without symmetry (herringbone-like) and another with  $C_i$  symmetry (parallel and herringbone-like, see Figure 1).

**3.2.1. Nonsymmetric Herringbone-like Dimer.** Table 3 shows the vertical energies, oscillator strengths, character of the states, modulus of the dipole moments, density difference plots, and natural orbitals with significant changes in occupation numbers of the five lowest-lying singlet excited electronic states of the herringbone-like pentacene dimer computed at the CASPT2/CASSCF/ANO-S-VDZP level of theory. The geometrical arrangement of this dimer is consistent with the directionality of the lowest-lying exciton found in the S-phase of solid pentacene.<sup>50,51</sup> As can be seen, all these states are close-lying in an energy window of  $\sim 0.3$  eV.  $S_1$  is an absorbing state that can be described mainly in terms of a CSF involving a single excitation. This state is of CT character with net charge separation between the pentacene moieties as indicated by its dipole moment, density difference plot and most significant CSF contributing to the wave function (see Table 3 and Table S3 in Supporting Information). The nature of this state is similar to that of the lowest-lying exciton found in the pentacene crystal.<sup>50,51</sup> However, a dimer model cannot accurately describe the degree of delocalization of the exciton in the solid, and therefore, the vertical excitation energy of this state is slightly higher ( $\sim 0.3$  eV) than the energy found for the exciton in the organic crystal.  $S_2$  is also a bright state that can be characterized mainly as a local single excitation in one pentacene moiety. In the dissociation limit, this state correspond to two pentacene units, one in the lowest-lying excited state and the other in the ground state. Therefore, we denote this state as locally excited (LE) state despite the fact that the excitation is slightly delocalized as shown by the density difference plots depicted in Table 3. This type of state is also referred to as Frenkel exciton state in the context of crystals. This LE state has certain amount of CT character as shown by the value of the dipole moment, the density difference plot and the weight of the CT CSFs (see Table S3 in Supporting Information).  $S_3$  is a dark state that can mainly be described in terms of doubly excited CSFs and, as can be seen in Table 3, shows very similar changes in the density in both pentacene moieties. In particular, the wave function of this state contains a 61% of ME character (see Table S3 in Supporting Information). An electronic state of this type may dissociate into two triplet states, each localized in a different pentacene moiety, and its population via fast internal conversion has been advocated as the main mechanism of SF.  $S_4$  is another dark CT state (see Table 3) that can again be described in terms of a CSF involving a single excitation. Finally,  $S_5$  is a bright LE state that exhibits a larger degree of CT than  $S_2$  as indicated by its

dipole moment and the amount of CT CSFs contained in its wave function (see Table S3 in Supporting Information). These results differ in the ordering of the states and their excitation energies from those recently reported in ref 48 obtained using the extended multiconfigurational quasidegenerate perturbation theory (XMCQDPT).<sup>7</sup> In particular, the authors of ref 48 found that the lowest-lying excited state is of ME character and its excitation energy is  $\sim 0.5$  eV red-shifted compared to the value obtained at the CASPT2 level. Furthermore, the energy difference between the two lowest-lying CT states also differs ( $\sim 0.8$  eV and  $\sim 0.33$  eV at the XMCQDPT and CASPT2 level, respectively). Possible reasons for these discrepancies are the different geometries considered and the smaller active space used in ref 48.

The GW/BSE results depicted in Table 4 for LE and CT states are in partial agreement with those obtained using

**Table 4. Vertical Excitation Energies (GW/BSE, in eV), Character of the States, and Most Significant Single Excitation Contributions of the Four Lowest-Lying Singlet Excited Electronic States of the Pentacene Herringbone Dimer**

State	$\Delta E$	Character	Most Significant	Single Excitations
$S_1$	1.92	CT		
$S_2$	2.38	LE		
$S_3$	2.40	LE		
$S_4$	2.60	CT		

CASPT2. In particular, both methods characterize the lowest-lying absorbing state as a CT state (although there is a difference in the excitation energy of about of 0.3 eV) and also predict the second excited state as a LE state. Differences appear for the higher lying LE and CT states that are well separated at the GW/BSE level but are near degenerate at the CASPT2 level. It is also interesting to note that both lowest-lying LE states are near degenerate at the GW/BSE level contrary to what happens at the CASPT2 level. This suggests that for this conformation the coupling is smaller at the GW/BSE level compared to CASPT2. Furthermore, the ME state ( $S_3$  at the CASPT2 level) is absent at the GW/BSE level of theory; however, as discussed above, this is expected and related to the limitations of the GW/BSE method for describing states with a significant contribution of doubly excited configurations.

**3.2.2. Symmetric Parallel Dimer.** Table 5 contains the vertical excitation energies, oscillator strengths, character of the states, density difference plots, and natural orbitals with significant changes in occupation numbers of the three lowest-lying singlet excited electronic states of the symmetric  $C_i$  pentacene dimer computed at the CASPT2/CASSCF/ANO-S-VDZP level of theory. For this conformation,  $S_1$  and  $S_2$

**Table 5.** Vertical Excitation Energies [CASPT2/SA-CASSCF(8,8)/ANO-S-VDZP, in eV], Oscillator Strengths, Character of the States, Density Difference Plots and Natural Orbitals with Significant Changes in Occupation Numbers of the Three Lowest-Lying Singlet Excited Electronic States of the Symmetric  $C_i$  Pentacene Dimer<sup>a</sup>

State	$\Delta E$	f	Character	Density Difference	Natural Orbitals
$S_1 (A_u)$	2.32	0.427	LE		
$S_2 (A_g)$	2.36	0.000	LE		
$S_3 (A_g)$	2.44	0.000	ME		

<sup>a</sup>Density differences and natural orbitals were computed at the SA-CASSCF(8,8)/ANO-S-VDZP level. In the density difference plots the yellow indicates accumulation and blue depletion of electronic density, respectively (an isolevel value of 0.0003 au was used in the plots).

are a bright state of  $A_u$  symmetry and a dark state of  $A_g$  symmetry, respectively. The wave functions of both states can be described in terms of two CSFs involving single excitations and with negligible contributions of CT configurations (see Table S4 in Supporting Information).  $S_3$  is a dark ME state of  $A_g$  symmetry. Similar to the  $S_3$  state found in the herringbone-like conformation, the wave function has a leading CSF of ME character. However, the weight of these contributions is larger in this conformation than in the herringbone-like case (77% vs 61%, see Tables S3 and S4 in Supporting Information), which indicates the existence of less mixing with other configurations and therefore less coupling with other states than in the herringbone-like case. The vertical excitation energies of the three lowest-lying states span an energy range that is within the typical accuracy of the method, and hence, they can be considered quasi-degenerate. In particular, the two LE states are closer in energy than the equivalent ones in the herringbone-like conformation, which indicates the existence of a larger coupling in the herringbone-like structure. This fact can be explained on the basis of the different geometrical conformations of both dimers. As shown in Figure 1, both pentacene units are displaced from each other in the  $C_i$  symmetric structure whereas the geometry of the herringbone-like dimer facilitates a better stacking interaction between the pentacene monomers, therefore increasing the coupling.

It is worth noting that for the symmetric  $C_i$  pentacene dimer CT states characterized by a net charge transfer from one of the monomers to the other cannot be expected as a result of the symmetry of the system. However, despite of the symmetry, CT CSFs may still contribute to the different electronic states as long as they do not result in a net dipole moment. In particular, for states  $S_4$  and  $S_6$  these CSFs are the dominant ones with weights ~90% (see Table S4 in Supporting Information). Contrary to the case of the herringbone-like dimer, these states are located relatively high in energy (3.03 and 3.04 eV, respectively) at the CASPT2 level.

The GW/BSE results are shown in Table 6. As for the herringbone dimer, there is rather good agreement with the CASPT2 results for the two lowest-lying excited states, which are predicted by both methods as locally excited states, with

**Table 6.** Vertical Excitation Energies (GW/BSE, in eV) and Most Significant Single Excitation Contributions of the Three Lowest-Lying Singlet Excited Electronic States of the Symmetric  $C_i$  Pentacene Dimer

State	$\Delta E$	Most Significant Single Excitations
$S_1$	2.36	
$S_2$	2.43	
$S_3$	2.45	

GW/BSE excitation energies slightly blue-shifted compared to the CASPT2 results. The main difference is seen in the third excited state,  $S_3$ . Whereas GW/BSE characterizes  $S_3$  as a locally excited state similar to  $S_1$ , CASPT2 identifies  $S_3$  as a ME state whose wave function involves several CSFs with doubly excited character.

The aforementioned results indicate that depending on the type of dimer model used to study the SF process CT states may (herringbone-like dimer or may not ( $C_i$  dimer) be present close to the absorbing state. On the other hand, the ME state is always found in both the symmetric and nonsymmetric dimers. To account for the delocalization character of the exciton in the pentacene solid and to investigate the effect that the system size has in the nature and ordering of the lowest-lying singlet excited states, we have analyzed several trimers of pentacene

consistent with the symmetry of the pentacene crystal (see Figure 1).

**3.2.3. Symmetric Herringbone-like Trimers.** We have studied two trimer conformations with herringbone-like motifs, HS-1 and HS-2, both exhibiting  $C_i$  symmetry and consistent with the directionality of the lowest-lying exciton found in the S-phase of the pentacene crystal. The results obtained for these systems are depicted in Tables 7 and 8, respectively.

**Table 7. Vertical Excitation Energies [CASPT2/SA-CASSCF(12,12)/ANO-S-VDZP, in eV], Oscillator Strengths, and Density Difference Plots of the Seven Lowest-Lying Singlet Excited Electronic States of the  $C_i$  HS-1 Herringbone-like Pentacene Trimer<sup>a</sup>**

State	$\Delta E$	f	Character	Density Difference
S <sub>1</sub> (A <sub>u</sub> )	2.10	0.248	LE	
S <sub>2</sub> (A <sub>u</sub> )	2.10	0.051	CT	
S <sub>3</sub> (A <sub>g</sub> )	2.21	0.000	LE/CT	
S <sub>4</sub> (A <sub>u</sub> )	2.23	0.166	LE/CT	
S <sub>5</sub> (A <sub>g</sub> )	2.39	0.000	CT	
S <sub>6</sub> (A <sub>u</sub> )	2.41	<0.001	ME	
S <sub>7</sub> (A <sub>g</sub> )	2.54	0.000	ME	

<sup>a</sup>Density differences were computed at the SA-CASSCF(12,12)/ANO-S-VDZP level. In the density difference plots, yellow indicates accumulation and blue depletion of electronic density, respectively (an isolevel value of 0.0003 au was used in the plots).

In the HS-1 trimer, the lowest-lying excited state, S<sub>1</sub>, is an absorbing state of A<sub>u</sub> symmetry with the excitation mainly localized in the central pentacene unit but also showing contributions in the lateral pentacene units (see Table 8). S<sub>1</sub> is degenerate with S<sub>2</sub>, a weakly absorbing state. S<sub>2</sub> is an intermolecular CT state that involves the redistribution of the electronic density from the central pentacene unit to the external ones. As expected for the point group symmetry of the system, this state, despite having net charge separation over the different pentacene units, has a vanishing static dipole moment. S<sub>3</sub>, S<sub>4</sub>, and S<sub>5</sub> are three close-lying excited states with different degrees of localization of the excitation and CT character. In particular, S<sub>3</sub> and S<sub>4</sub> are well described in terms of CSFs

**Table 8. Vertical Excitation Energies [CASPT2/SA-CASSCF(12,12)/ANO-S-VDZP, in eV], Oscillator Strengths and Density Difference Plots of the Seven Lowest-Lying Singlet Excited Electronic States of the  $C_i$  HS-2 Herringbone-like Pentacene Trimer<sup>a</sup>**

State	$\Delta E$	f	Character	Density Difference
S <sub>1</sub> (A <sub>u</sub> )	1.83	0.104	CT	
S <sub>2</sub> (A <sub>g</sub> )	2.19	0.000	CT	
S <sub>3</sub> (A <sub>g</sub> )	2.27	0.000	LE/CT	
S <sub>4</sub> (A <sub>u</sub> )	2.28	0.341	LE/CT	
S <sub>5</sub> (A <sub>u</sub> )	2.34	0.072	LE/CT	
S <sub>6</sub> (A <sub>u</sub> )	2.55	<0.001	ME	
S <sub>7</sub> (A <sub>g</sub> )	2.67	0.000	ME	

<sup>a</sup>Density differences were computed at the SA-CASSCF(12,12)/ANO-S-VDZP level. In the density difference plots, yellow indicates accumulation and blue depletion of electronic density, respectively (an isolevel value of 0.0003 au was used in the plots).

involving single excitations. These states also exhibit some CT character, as can be observed in the density difference plot. This is significant for the SF process, as the presence of CT CSFs in the wave function may facilitate the coupling of these states to the ME state.<sup>41,42</sup> S<sub>5</sub> can be clearly characterized as an intermolecular CT state (see the density difference plot in Table 8). Finally, S<sub>6</sub> and S<sub>7</sub> are dark states which show significant contributions of doubly excited CSFs. In particular, the density difference plot of S<sub>7</sub> resembles that of the ME state found in the herringbone-like dimer.

The results obtained for the HS-2 trimer differ from those found for HS-1 (see Table 8). In particular, S<sub>1</sub> is an absorbing state of A<sub>u</sub> symmetry. Interestingly, its vertical excitation energy (1.83 eV) and its CT character correspond to those found for the lowest-lying exciton in the S-phase crystal structure of pentacene.<sup>50,51</sup> S<sub>2</sub> is a dark state of A<sub>g</sub> symmetry and CT character. S<sub>3</sub>, S<sub>4</sub>, and S<sub>5</sub> are three near degenerate electronic excited states with different degrees of localization of the excitation and CT character, as can be observed in the density difference plots depicted in Table 8. Specifically, S<sub>4</sub> is a bright

state of  $A_u$  symmetry where the excitation is localized in the external pentacene units of the trimer. The contribution of CT CSFs to the wave function of this state may facilitate the SF process enhancing the coupling between this state and the ME state of  $^1(T_1T_1)$  type leading to SF, as in HS-1.  $S_3$  is a dark state of  $A_g$  symmetry with partial CT character and  $S_5$  is a weak absorbing state of  $A_u$  symmetry, where the excitation is mainly localized in the central pentacene unit of the trimer, although some significant delocalization over the whole system can be observed. Compared with the equivalent states in the HS-1 trimer, they show different order and energies, which is a consequence of the different interaction existing among the pentacenes due to the different geometrical conformations of both herringbone-like trimers. This ultimately affects the couplings between states, in particular modifying the weight of CT contributions in the wave functions of the different electronic states. Finally,  $S_6$  and  $S_7$  are, as in the case of HS-1, dark states with multiconfigurational character and with wave functions showing significant contributions of doubly excited CSFs. In particular,  $S_7$  as in the case of HS-1, closely resembles the ME state found in the herringbone-like dimer as the density difference plot shows. The order of these states is reverse to that found in HS-1 but, similar to the HS-1 case, these states are significantly higher in energy than those with appreciable oscillator strength.

**3.2.4. Symmetric Parallel-like Trimer.** The lowest-lying singlet excited electronic states vertical excitation energies obtained for the  $C_i$  parallel-like trimer and their density differences are shown in Table 9. The nature of the lowest-lying electronic excited states of this trimer conformation is similar to that of the states of the herringbone-like trimers. However, several points are worth noting. First, and contrary to the case of the parallel  $C_i$  dimer, there are low-lying electronic states in the range of energies of interest ( $S_4$ ,  $S_5$ , and  $S_6$ ) with significant intermolecular CT character (see Table 9). Second, both the CT ( $S_4$ ,  $S_5$ , and  $S_6$ ) and the ME ( $S_7$ , see Table 9) states are higher in energy than the lowest-lying absorbing state  $S_3$ . Specifically, the differences in energy with respect to the bright state is for the CT states 0.09 eV ( $S_4$ ), 0.15 eV ( $S_5$ ), and 0.34 eV ( $S_6$ ) and 0.35 eV for the ME state ( $S_7$ ). Population of the lowest-lying absorbing excited state ( $S_3$ ) would provide a possible pathway for SF via a CT-state mediated mechanism, as the energy difference with respect to the lowest-lying CT state ( $S_4$ ) is very small (0.09 eV) and only a minimal geometrical deformation of the absorbing state would be needed for a state crossing. Similarly to HS-1 and HS-2, the ME state ( $S_7$ ) exhibits a pronounced energy difference with respect to the bright state, which indicates that significant geometry relaxation in the absorbing state is needed to facilitate SF upon population of  $S_3$ .

**3.3. Discussion of the Results in the Context of Singlet Fission.** The results show that in all trimer systems investigated there are CT states that are energetically close to the bright states. Specifically, in HS-1 the CT state  $S_2$  is degenerate with the bright state whereas in HS-2 the CT state  $S_1$  is even more stable than the absorbing states which themselves exhibit some CT character. A similar situation is also found in the  $C_i$  parallel-like conformation, where  $S_4$  is nearly degenerate with the absorbing state. Thus, the first step in a two-step SF mechanism of the type



that is, the formation of a CT state after photoexcitation of the bright state (BS, that could itself be a CT state formed through

**Table 9. Vertical Excitation Energies [CASPT2/SA-CASSCF(12,12)/ANO-S-VDZP, in eV], Oscillator Strengths and Density Difference Plots of the Seven Lowest-Lying Singlet Excited Electronic States of the  $C_i$  Parallel-like Pentacene Trimer<sup>a</sup>**

State	$\Delta E$	f	Character	Density Difference
$S_1 (A_g)$	2.07	0.000	LE	
$S_2 (A_u)$	2.11	<0.001	LE	
$S_3 (A_u)$	2.19	0.600	LE	
$S_4 (A_g)$	2.28	0.000	CT	
$S_5 (A_u)$	2.34	<0.001	CT	
$S_6 (A_g)$	2.53	0.000	CT	
$S_7 (A_g)$	2.54	0.000	ME	

<sup>a</sup>Density differences were computed at the SA-CASSCF(12,12)/ANO-S-VDZP level. In the density difference plots, yellow indicates accumulation and blue depletion of electronic density, respectively (an isolevel value of 0.0003 au was used in the plots).

a photoinduced charge separation as possibly  $S_1$  in HS-2) is energetically possible. However, the results also reveal that, in all trimers considered, the ME state has a significantly higher energy than the absorbing states ( $\sim 0.3\text{--}0.7$  eV). Therefore, the second step in the two-step schema, eq 3, that is, the transition from the CT to the ME state, requires significant geometry reorganization. The same argument also applies for the direct transition from the bright state to the ME state in the direct SF mechanism



In the dimer structures, the bright state is also located lower in energy than the ME state, but the difference is smaller ( $\sim 0.1$  eV) than in the trimer structures. This is due to the fact that the bright states are stabilized upon increase of the system size, while the energy of the ME states is less sensitive to this.

Assuming photoexcitation to the lowest bright state, the results obtained in this paper suggest that the two-step mechanism via a CT state (that is, a state that may or may not exhibit a permanent dipole moment but whose wave

function is expressed mainly in terms of CT CSFs) can be an important pathway for SF. This situation may be different for photoexcitation to higher lying absorbing states, where the ME state is energetically directly accessible. A detailed investigation of the contributions of the different pathways requires the explicit simulation of the nonadiabatic photodynamics in these system, which will be the subject of future work.

#### 4. CONCLUSIONS

We have investigated the lowest-lying electronically excited states in pentacene oligomers employing two different electronic structure methods, CASPT2/CASSCF and GW/BSE. While the former method can provide accurate benchmark results for smaller oligomers and a balanced treatment of electronic states of very different character, the latter method is straightforwardly applicable to solids, for example, pentacene crystals.

The results obtained for dimers and trimers with different geometries reveal the complex electronic structure, which includes LE states with different degrees of CT contributions, CT states (that do or do not exhibit a permanent dipole moment but with wave functions characterized by dominant CT CSFs), and ME states with different degrees of  ${}^1(T_1T_1)$  character. The use of trimers of pentacene allows an improved description of the delocalized character of the lowest-lying exciton found in the S-phase of solid pentacene. Furthermore, it provides a characterization of the lowest-lying singlet electronic states in different geometrical conformations consistent with the symmetry of the pentacene crystal. In all trimers investigated, the ME states are located relatively high in energy, while CT states exist in close proximity to the lowest-lying absorbing states. In the context of SF, this suggests that a two-step mechanism via CT states is energetically possible. The transition from the bright or the CT state to the ME state, on the other hand, requires geometry reorganization.

From the point of view of methodology, the results show that the GW/BSE methodology provides a description of LE and CT states, and therefore of the absorption spectrum, comparable to that obtained with CASPT2. To describe dark ME states and their role in the SF process, on the other hand, the current implementation of the method has to be extended to include double excitations.<sup>72</sup>

#### ■ ASSOCIATED CONTENT

##### Supporting Information

Further details on the electronic structure calculations and Cartesian coordinates of all systems investigated in this work. This material is available free of charge via the Internet at <http://pubs.acs.org/>.

#### ■ AUTHOR INFORMATION

##### Corresponding Authors

\*E-mail: pedro.brana-coto@physik.uni-erlangen.de.  
\*E-mail: ssharifzadeh@lbl.gov.  
\*E-mail: jbneaton@lbl.gov.  
\*E-mail: michael.thoss@physik.uni-erlangen.de.

##### Present Address

<sup>#</sup>Department of Electrical and Computer Engineering and Division of Materials Science and Engineering, Boston University, Boston, MA 02215.

##### Notes

The authors declare no competing financial interest.

#### ■ ACKNOWLEDGMENTS

This work has been supported by the FAU Erlangen-Nürnberg within the Emerging Field Initiative (EFI), the Deutsche Forschungsgemeinschaft (DFG) through the Clusters of Excellence “Engineering of Advanced Materials” (EAM), and the U.S. Department of Energy, Office of Basic Energy Sciences and of Advanced Scientific Computing Research through the SciDAC Program on Excited State Phenomena. Portions of this work took place at the Molecular Foundry, supported by the U.S. Department of Energy, Office of Basic Energy Sciences. GW/BSE calculations were performed using computational resources from the National Energy Research Scientific Computing (NERSC) center, which is supported by the Office of Science of the U.S. Department of Energy under Contract No. DE-AC02-05CH11231. M.T. thanks the Chemistry Department at the University of California, Berkeley, for a visiting Pitzer Professorship and W. H. Miller (UC Berkeley) and J. Neaton (Molecular Foundry, LBNL) for their hospitality. The authors thank T. Fauster, D. M. Guldi, and R. Tykwnsky for inspiring and helpful discussions. Generous allocation of computing time at the computing centers in Erlangen (RRZE), Munich (LRZ), and Jülich (JSC) is gratefully acknowledged.

#### ■ REFERENCES

- (1) Smith, M. B.; Michl, J. *Chem. Rev.* **2010**, *110*, 6891–6936.
- (2) Smith, M. B.; Michl, J. *Annu. Rev. Phys. Chem.* **2013**, *64*, 361–386.
- (3) Paci, I.; Johnson, J. C.; Chen, X.; Rana, G.; Popović, D.; David, D. E.; Nozik, A. J.; Ratner, M. A.; Michl, J. *J. Am. Chem. Soc.* **2006**, *128*, 16546–16553.
- (4) Hanna, M. C.; Nozik, A. J. *J. Appl. Phys.* **2006**, *100*, 074510.
- (5) Thorsmølle, V.; Averitt, R.; Demsar, J.; Smith, D.; Tretiak, S.; Martin, R.; Chi, X.; Crone, B.; Ramirez, A.; Taylor, A. *Phys. Rev. Lett.* **2009**, *102*, 017401.
- (6) Rao, A.; Wilson, M. W. B.; Albert-Seifried, S.; Di Pietro, R.; Friend, R. H. *Phys. Rev. B* **2011**, *84*, 195411.
- (7) Wilson, M. W. B.; Rao, A.; Clark, J.; Kumar, R. S. S.; Brida, D.; Cerullo, G.; Friend, R. H. *J. Am. Chem. Soc.* **2011**, *133*, 11830–11833.
- (8) Chan, W.-L.; Ligges, M.; Zhu, X.-Y. *Nat. Chem.* **2012**, *4*, 840–845.
- (9) Congreve, D. N.; Lee, J.; Thompson, N. J.; Hontz, E.; Yost, S. R.; Reusswig, P. D.; Bahlke, M. E.; Reineke, S.; Van Voorhis, T.; Baldo, M. A. *Science* **2013**, *340*, 334–337.
- (10) Lee, J.; Jadhav, P.; Reusswig, P. D.; Yost, S. R.; Thompson, N. J.; Congreve, D. N.; Hontz, E.; Van Voorhis, T.; Baldo, M. A. *Acc. Chem. Res.* **2014**, *46*, 1300–1311.
- (11) Wilson, M. W. B.; Rao, A.; Ehrler, B.; Friend, R. H. *Acc. Chem. Res.* **2013**, *46*, 1330–1338.
- (12) Walker, B. J.; Musser, A. J.; Beljonne, D.; Friend, R. H. *Nat. Chem.* **2013**, *5*, 1019–1024.
- (13) Shockley, W.; Queisser, H. J. *J. Appl. Phys.* **1961**, *32*, 510–519.
- (14) Singh, S.; Jones, W. J.; Siebrand, W.; Stoicheff, B. P.; Schneider, W. G. *J. Chem. Phys.* **1965**, *42*, 330–342.
- (15) Merrifield, R.; Avakian, P.; Groff, R. *Chem. Phys. Lett.* **1969**, *3*, 155–157.
- (16) Geacintov, N.; Pope, M.; Vogel, F. *Phys. Rev. Lett.* **1969**, *22*, 593–596.
- (17) Groff, R. P.; Avakian, P.; Merrifield, R. E. *Phys. Rev. B* **1970**, *1*, 815–817.
- (18) Geacintov, N.; Burgos, J.; Pope, M.; Strom, C. *Chem. Phys. Lett.* **1971**, *11*, 504–508.
- (19) Yarmus, L.; Rosenthal, J.; Chopp, M. *Chem. Phys. Lett.* **1972**, *16*, 477–481.
- (20) Schwob, H. P.; Williams, D. F. *J. Chem. Phys.* **1973**, *58*, 1542–1547.
- (21) Burgos, J.; Pope, M.; Swenberg, C. E.; Alfano, R. R. *Phys. Status Solidi B* **1977**, *83*, 249–256.

- (22) von Burg, K.; Zschokke-Granacher, I. *J. Chem. Phys.* **1979**, *70*, 3807–3811.
- (23) Agostini, G.; Corvaja, C.; Giacometti, G.; Pasimeni, L. *Chem. Phys.* **1993**, *173*, 177–186.
- (24) Jundt, C.; Klein, G.; Sipp, B.; Moigne, J. L.; Joucla, M.; Villaey, A. *Chem. Phys. Lett.* **1995**, *241*, 84–88.
- (25) Swenberg, C.; Stacy, W. *Chem. Phys. Lett.* **1968**, *2*, 327–328.
- (26) Suna, A. *Phys. Rev. B* **1970**, *1*, 1716–1739.
- (27) Swenberg, C.; van Metter, R.; Ratner, M. *Chem. Phys. Lett.* **1972**, *16*, 482–485.
- (28) Swenberg, C. E.; Ratner, M. A.; Geacintov, N. E. *J. Chem. Phys.* **1974**, *60*, 2152–2157.
- (29) Klein, G. *Chem. Phys. Lett.* **1978**, *57*, 202–206.
- (30) Greysen, E. C.; Stepp, B. R.; Chen, X.; Schwerin, A. F.; Paci, I.; Smith, M. B.; Akdag, A.; Johnson, J. C.; Nozik, A. J.; Michl, J.; Ratner, M. A. *J. Phys. Chem. B* **2010**, *114*, 14223–14232.
- (31) Minami, T.; Ito, S.; Nakano, M. *J. Phys. Chem. Lett.* **2012**, *3*, 2719–2723.
- (32) Minami, T.; Ito, S.; Nakano, M. *J. Phys. Chem. Lett.* **2013**, *4*, 2133–2137.
- (33) Akdag, A.; Havlas, Z.; Michl, J. *J. Am. Chem. Soc.* **2012**, *134*, 14624–14631.
- (34) Greysen, E. C.; Vura-Weis, J.; Michl, J.; Ratner, M. A. *J. Phys. Chem. B* **2010**, *114*, 14168–14177.
- (35) Zimmerman, P. M.; Zhang, Z.; Musgrave, C. B. *Nat. Chem.* **2010**, *2*, 648–652.
- (36) Zimmerman, P. M.; Bell, F.; Casanova, D.; Head-Gordon, M. *J. Am. Chem. Soc.* **2011**, *133*, 19944–19952.
- (37) Havenith, R. W.; de Gier, H. D.; Broer, R. *Mol. Phys.* **2012**, *110*, 2445–2454.
- (38) Teichen, P. E.; Eaves, J. D. *J. Phys. Chem. B* **2012**, *116*, 11473–11481.
- (39) Zimmerman, P. M.; Musgrave, C. B.; Head-Gordon, M. *Acc. Chem. Res.* **2013**, *46*, 1339–1347.
- (40) Renaud, N.; Sherratt, P. A.; Ratner, M. A. *J. Phys. Chem. Lett.* **2013**, *4*, 1065–1069.
- (41) Berkelbach, T. C.; Hybertsen, M. S.; Reichman, D. R. *J. Chem. Phys.* **2013**, *138*, 114102.
- (42) Berkelbach, T. C.; Hybertsen, M. S.; Reichman, D. R. *J. Chem. Phys.* **2013**, *138*, 114103.
- (43) Chan, W.-L.; Berkelbach, T. C.; Provorse, M. R.; Monahan, N. R.; Tritsch, J. R.; Hybertsen, M. S.; Reichman, D. R.; Gao, J.; Zhu, X.-Y. *Acc. Chem. Res.* **2013**, *46*, 1321–1329.
- (44) Beljonne, D.; Yamagata, H.; Brédas, J. L.; Spano, F. C.; Olivier, Y. *Phys. Rev. Lett.* **2013**, *110*, 226402.
- (45) Feng, X.; Luzanov, A. V.; Krylov, A. I. *J. Phys. Chem. Lett.* **2013**, *4*, 3845–3852.
- (46) Akimov, A. V.; Prezhdo, O. V. *J. Am. Chem. Soc.* **2014**, *136*, 1599–1608.
- (47) Kolomeisky, A. B.; Feng, X.; Krylov, A. I. *J. Phys. Chem. C* **2014**, *118*, 5188–5195.
- (48) Zeng, T.; Hoffmann, R.; Ananth, N. *J. Am. Chem. Soc.* **2014**, DOI: 10.1021/ja500887a.
- (49) Casanova, D. *J. Chem. Theory Comput.* **2014**, *10*, 324–334.
- (50) Sharifzadeh, S.; Biller, A.; Kronik, L.; Neaton, J. B. *Phys. Rev. B* **2012**, *85*, 125307.
- (51) Sharifzadeh, S.; Darancet, P.; Kronik, L.; Neaton, J. B. *J. Phys. Chem. Lett.* **2013**, *4*, 2197–2201.
- (52) Roos, B. O.; Fülscher, M. P.; Malmqvist, P.-Å.; Merchán, M.; Serrano-Andrés, L. *Adv. Chem. Phys.* **1996**, *93*, 219–331.
- (53) Hybertsen, M. S.; Louie, S. G. *Phys. Rev. B* **1986**, *34*, 5390–5413.
- (54) Rohlfing, M.; Louie, S. G. *Phys. Rev. B* **2000**, *62*, 4927–4944.
- (55) Perdew, J. P.; Ernzerhof, M.; Burke, K. *J. Chem. Phys.* **1996**, *105*, 9982–9985.
- (56) Giannozzi, P.; Baroni, S.; Bonini, N.; Calandra, M.; Car, R.; Cavazzoni, C.; Ceresoli, D.; Chiarotti, G. L.; Cococcioni, M.; Dabo, I.; Dal Corso, A.; de Gironcoli, S.; Fabris, S.; Fratesi, G.; Gebauer, R.; Gerstmann, U.; Gougaussis, C.; Kokalj, A.; Lazzeri, M.; Martin-Samos,
- L.; Marzari, N.; Mauri, F.; Mazzarello, R.; Paolini, S.; Pasquarello, A.; Paulatto, L.; Sbraccia, C.; Scandolo, S.; Scaluzero, G.; Seitsonen, A. P.; Smogunov, A.; Umari, P.; Wentzcovitch, R. M. *J. Phys.: Condens. Matter* **2009**, *21*, 395502.
- (57) Troullier, N.; Martins, J. L. *Phys. Rev. B* **1991**, *43*, 1993–2006.
- (58) Deslippe, J.; Samsonidze, G.; Strubbe, D. A.; Jain, M.; Cohen, M. L.; Louie, S. G. *Comput. Phys. Commun.* **2012**, *183*, 1269–1289.
- (59) Widmark, P.-O.; Malmqvist, P.-Å.; Roos, B. O. *Theor. Chim. Acta* **1990**, *77*, 291–306.
- (60) Pierloot, K.; Dumez, B.; Widmark, P.-O.; Roos, B. O. *Theor. Chim. Acta* **1995**, *90*, 87–114.
- (61) Ghigo, G.; Roos, B. O.; Malmqvist, P.-Å. *Chem. Phys. Lett.* **2004**, *396*, 142–149.
- (62) Forsberg, N.; Malmqvist, P.-Å. *Chem. Phys. Lett.* **1997**, *274*, 196–204.
- (63) Aquilante, F.; De Vico, L.; Ferré, N.; Ghigo, G.; Malmqvist, P.-Å.; Neogrády, P.; Pedersen, T. B.; Pitonák, M.; Reiher, M.; Roos, B. O.; Serrano-Andrés, L.; Urban, M.; Veryazov, V.; Lindh, R. *J. Comput. Chem.* **2010**, *31*, 224–247.
- (64) Onida, G.; Reining, L.; Rubio, A. *Rev. Mod. Phys.* **2002**, *74*, 601–659.
- (65) Heinecke, E.; Hartmann, D.; Müller, R.; Hese, A. *J. Chem. Phys.* **1998**, *109*, 906–911.
- (66) Halasinski, T. M.; Hudgins, D. M.; Salama, F.; Allamandola, L. J.; Bally, T. *J. Phys. Chem. A* **2000**, *104*, 7484–7491.
- (67) Grimme, S.; Parac, M. *ChemPhysChem* **2003**, *4*, 292–295.
- (68) Parac, M.; Grimme, S. *Chem. Phys.* **2003**, *292*, 11–21.
- (69) Marian, C. M.; Gilka, N. *J. Chem. Theory Comput.* **2008**, *4*, 1501–1515.
- (70) Knippenberg, S.; Starcke, J. H.; Wormit, M.; Dreuw, A. *Mol. Phys.* **2010**, *108*, 2801–2813.
- (71) Granovsky, A. A. *J. Chem. Phys.* **2011**, *134*, 214113.
- (72) Sangalli, D.; Romaniello, P.; Onida, G.; Marini, A. *J. Chem. Phys.* **2011**, *134*, 034115.